

WACODI: A generic algorithm to derive the intrinsic color of natural waters from digital images

Stéfani Novoa,*¹ Marcel Wernand,¹ Hendrik Jan van der Woerd²

¹Royal Netherlands Institute for Sea Research, Physical Oceanography, Marine Optics & Remote Sensing, Den Burg, Texel, Netherlands

²Department of Biology and Chemistry, Institute for Environmental Studies (IVM), VU University Amsterdam, Amsterdam, Netherlands

Abstract

This document presents the Water Color from Digital Images (WACODI) algorithm, which extracts the color of natural waters from images collected by low-cost digital cameras, in the context of participatory science and water quality monitoring. SRGB images are converted to the CIE XYZ color space, undergoing a gamma expansion and illumination correction that includes the specular reflection at the air-water interface. The XYZ values obtained for each pixel of the image are converted to chromaticity coordinates and Hue color angle (α_w), which is a measure of color. Based on the distributions of α_w in sub-sections of the image, an approximation of the intrinsic color of the water is obtained. This algorithm was applied to images acquired in 2013 during two field campaigns in Northern Europe. The Hue color angles were derived from hyperspectral measurements above and below the surface, carried out simultaneously with image acquisition. When for each station a specific illumination correction was applied, based on the corresponding hyperspectral data, a good fit ($r^2 = 0.93$) was obtained between the image and the spectra Hue color angles (slope = 0.98, intercept = -0.03). When a more generic illumination correction was applied to the same images, based on the sky conditions at the time of the image acquisition (either overcast or sunny), a slightly inferior, but still satisfactory fit resulted. Results on the application of the WACODI algorithm to the first images collected by the public via the smartphone application or “APP,” developed within the European FP7 Citclops, are presented at the end of this study.

One commonly adopted scientific approach to assess the environmental status of water bodies is by measuring their optical properties. Together with water clarity, the color of natural waters is the most apparent optical property of natural water. Changes in these optical properties in aquatic systems can be due to natural causes, such as plankton blooms, river outflows (transport of organic materials, nutrients and minerals) and changing meteorological conditions or can be linked to anthropogenic activities. For instance, the introduction of an excess of nutrients originating from fertilisers used in agriculture can cause algal proliferations (Anderson et al. 2002; Heisler et al. 2008) that affect the color and

clarity of the water. This phenomenon is known as eutrophication, which is a major environmental issue across Europe (Bøgestrand et al. 2005; Ferreira et al. 2011). To determine if a change in color is due to a particular anthropogenic activity, it is important to collect long-term data on the color and clarity of water bodies (British Columbia Ministry of Environment 1999). To facilitate this goal, it is necessary to develop citizen engaging tools to obtain high sampling frequencies and to cover large areas.

The intrinsic color of natural waters is determined by the spectral characteristics and the concentrations of dissolved and suspended colored compounds (IOCCG 2000, 2008). There are three main components that alter the color of oceanic, coastal and continental waters: (1) colored dissolved organic matter (CDOM), (2) sediment load (total suspended material, TSM) and (3) gross biological activity (estimated generally through the chlorophyll *a* concentration, Chl *a*). These components are important water quality indicators (IOCCG 2000, 2008) and commonly monitored for the larger areas, by means of optical satellite remote sensing of the

Additional Supporting Information may be found in the online version of this article.

*Correspondence: snovoa@gmail.com

This is an open access article under the terms of the Creative Commons Attribution-NonCommercial License, which permits use, distribution and reproduction in any medium, provided the original work is properly cited and is not used for commercial purposes.

ocean (oceancolor.gsfc.nasa.gov), coastal areas (www.coast-color.org) and even lakes (http://www.globolakes.ac.uk), since they affect water transparency, a parameter that needs to be monitored in coastal areas to comply with the European water directives (2006/7/EC; 2008/56/EC; 2000/60/EC). However, even if the satellite spatial resolution is improving and it is suitable for the open ocean, it is less accurate in coastal and inland waters (Blondeau-Patissier et al. 2004; Gohin et al. 2005). Relatively complex radiometers, airborne or at ground level, are used to improve the resolution and are used to validate satellite images (Kallio et al. 2001; Deschamps et al. 2004; Nechad et al. 2010). However, these actions are expensive and laborious.

The Forel-Ule scale (Ule 1894; Forel 1895) has been applied globally and intensively by oceanographers and limnologists to determine the color of natural waters since the 19th century, providing one of the oldest oceanographic datasets. The Forel-Ule scale is composed of 21 color standards varying between blue-green and brown. Wernand et al. (2013a) used these datasets to estimate global changes occurring in the ocean in relation to the Chl *a* concentration, a key index of phytoplankton biomass and primary productivity studies. For coastal and inland waters more optically active constituents determine the water leaving radiance and color (IOCCG 2000; van der Woerd and Pasterkamp 2008). Wernand et al. (2013b) developed a specific MERIS algorithm (named FUME) to determine the color of natural water, based on color angles (α_w) converted to the Forel-Ule index FU (Ule 1892; Forel 1895; Wernand and van der Woerd 2010; Novoa et al. 2013; Wernand et al. 2013a,b). The application of this algorithm to satellite images allows classifying the seas and oceans based on their color.

Observations of ocean color has made much progress since the deployment of satellites. Ocean color science utilizes the apparent color of natural waters to derive concentrations of different components, important for a wide range of oceanographic studies, such as long-term monitoring of water quality indicators (Hu et al. 2004; Giardino et al. 2007; Tudesque et al. 2008; Van der Woerd and Pasterkamp 2008; Novoa et al. 2012). In ocean color science, the intrinsic color of the water surface is estimated by correcting the effect of the sky reflection and light penetration on the water column by means of spectral measurements of the sky irradiance (Mobley 1999; Mueller et al. 2003). In this study, we combined concepts and techniques used in satellite imagery with the science of colors, as described by the ICC (2014), to develop the WACODI algorithm. Colorimetry is the brand of science used to quantify and describe physically the human color perception. It is distinguished from spectrophotometry by its interest in reducing spectra to the physical correlates of color perception such as the CIE 1931 XYZ color space tristimulus values and standardizes the illumination correction. Previous studies have applied colorimetric techniques

to assess water color changes in water bodies (Smith et al. 1973; Smith and Baker 1977; Davies-colley et al. 1997) and used digital imaging to estimate water quality indicators (Goddijn-Murphy et al. 2009; Hoguane et al. 2012). In this study, the novelty resides in the combination of spectrometric and colorimetric techniques to extract the intrinsic color of natural waters from digital images.

FU estimates have a historical background and have been shown to be related to water quality indicators, such as Chl *a*, CDOM and SPM (Wernand et al. 2013a), but also represent an easy and fast method for citizen's to estimate the color of water bodies. Davies-Colley et al. (1997, 1993) showed that a color-matching method is suitable for routine water resources surveys and monitoring, as humans can easily match colors observed simultaneously. In addition, acquiring a large amount of data through citizen participation and over an extended period of time, combined with a good implementation system, will provide a background on the color of aquatic bodies. The purpose of using FU index in coastal waters is to provide a simple standard way to monitor the color of aquatic systems. Then, color alterations in these water bodies could be considered as indicators of changes occurring in these environments, and could therefore be examined in further detail.

Therefore, the objective of this document is to present an algorithm able to extract the color from images of a water body based on the original FUME algorithm, with additional necessary procedures (i.e., illumination correction, gamma expansion and sub-image selection) and recommendations. This WACODI algorithm was assessed on RGB digital images acquired during two field campaigns; one was undertaken in the North Sea and the other in coastal waters, lakes and rivers across the Netherlands. The proposed algorithm will be able to estimate the color of natural waters from images acquired by the public, i.e., citizens using smart phones or low-cost digital cameras. Data collection is part of the EC-funded CITLOPS project (Citizens' Observatory for Coast and Ocean Optical Monitoring; www.citclops.eu). The first results on the application of the algorithm on images acquired using different smartphones sent by the volunteers are finally shown.

Field campaigns

A total of 43 sampling stations were visited during two field campaigns; one in the North Sea ($n = 27$) in March 2013, for 11 d, and the other, a 5 d campaign covering Dutch coastal and continental water bodies in August 2013 ($n = 16$). The North Sea campaign was carried out along the East Anglia plume, where the water type is considered to be coastal due to the high suspended material concentrations generally present in the area (McManus and Prandle 1997; Dyer and Moffat 1998; Eleveld et al. 2008). The stations across the Netherlands were located in coastal areas, rivers

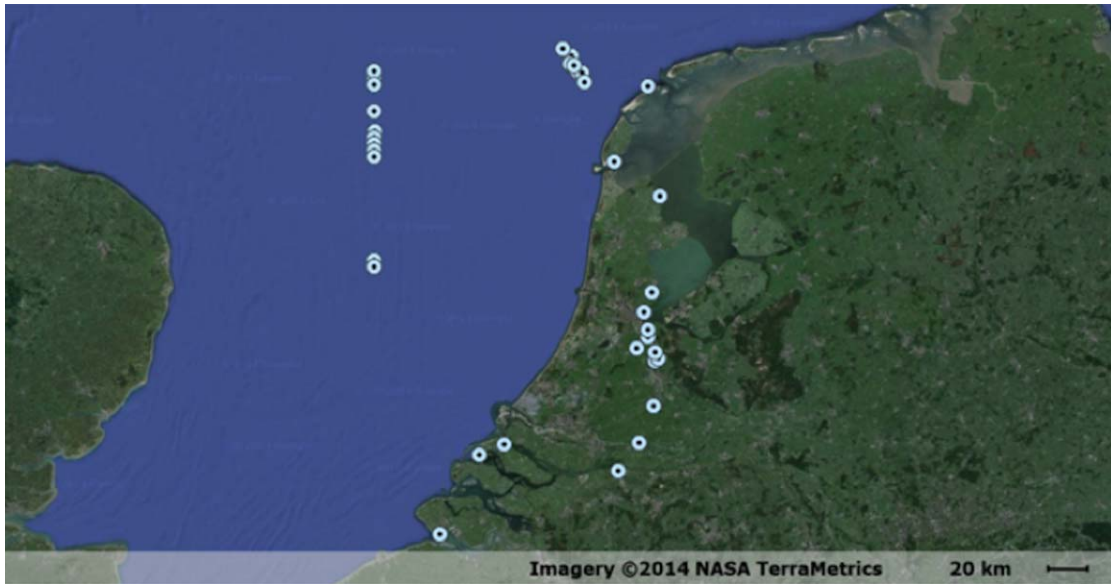


Fig. 1. Map showing the location of the sampling stations in the North Sea and across The Netherlands.

and lakes (Fig. 1) with varying composition resulting in green to dark brown colored waters.

Water samples were collected to determine concentrations of Chl *a* and total suspended material (TSM) and the light absorption by colored dissolved organic material (CDOM), following the protocols for the determination of inherent optical properties of natural waters (Tilstone et al. 2002). Water samples were collected at 0.5 m depth and directly filtered with GF/F filters. The Chl *a* extraction and analysis was achieved by HPLC for the North Sea stations following the protocols developed by Jeffrey and Vesk (1997). For the Dutch inland and coastal stations Chl *a* was estimated using spectrophotometry, following EPA’s protocols (Arar 1997). The TSM concentration was determined by the gravimetric method following the protocols established by Tilstone et al. (2002) and Van der Linden (1998). Water samples were collected, filtered with pre-weighed and pre-ashed GF/F filters (0.7 μm), and rinsed with milli-Q water. After the field work, the filters were dried and weighed for determination of TSM dry weight. For CDOM determination the GF/F filtrate of each station was again filtered over filters with 0.2 μm average pore size. Light attenuation of the filtrate in a 5 cm cuvette was analysed with a TriOS Vis-Spec analyser (320–950 nm).

At each station hyperspectral measurements were carried out using TriOS-RAMES radiometers following the NASA protocols (Mueller et al. 2003). The measurements included sky radiance (L_{sky}), upwelling radiance (L_{sfc}) and incident spectral irradiance (E_s). For calm inland waters, an additional radiance measurement was carried out just below (5–10 cm) the water surface. The radiometers cover the spectral range 320–950 nm with a spectral resolution of 3.3 nm (full width

at half maximum) and an accuracy of 0.3 nm. Multiple spectral measurements were carried out at each station and averaged per station. Radiance measurements were collected at an azimuth angle of 135° away from the Sun. Sky and water surface radiance were measured at 35° off zenith and nadir, respectively. As radiance measurements were collected with a viewing angle of 7° we stayed within limits of the recommended nadir angle of 40° (Mobley 1999; Mueller et al. 2003) and well below the Brewster angle.

The water-leaving radiance $L_W(\lambda, 0^+)$ at wavelength (λ) just above the surface (0^+) is derived from the following:

$$L_W(\lambda, 0^+) = L_{sfc}(\lambda, 0^+) - \rho \cdot L_{sky}(\lambda) \quad (1)$$

The reflectance factor ρ is a correction factor to compensate for Fresnel reflectance at the air/water boundary (Mueller et al. 2003), defined as the fraction of skylight actually reflected from the wave roughened (sea) surface. The intrinsic color of the water is determined by the spectral distribution of the remote-sensing reflectance $R_{RS}(\lambda, 0^+)$ that is calculated as the ratio of water-leaving radiance $L_W(\lambda, 0^+)$ to downwelling irradiance $E_s(\lambda, 0^+)$:

$$R_{RS} = L_W(\lambda, 0^+)/E_s(\lambda, 0^+) \quad (2)$$

During both campaigns, the Samsung EK-GC100 was used to take photographs of the waters under investigation. The camera looked to the water surface in the same direction as the spectrometers at nadir angle between 0° and 40° and at azimuth angle of approximately 135° away from the sun to avoid sun glint, following NASA’s recommendations for radiometric field measurements (Mueller et al. 2003). The Galaxy camera provides images in JPEG format.

Illumination conditions varied considerably during both campaigns due to the time of observation, the local weather conditions and water surface roughness. The cloud cover varied from overcast, to partial cloud cover, to sunny skies. Considerable differences in wind strength were found during the North Sea campaign, from 1 m s^{-1} to 25 m s^{-1} . Only the sea stations sampled during calm wind and sea conditions are included in this analysis.

Algorithm description

Digital imaging

It has been shown that digital cameras providing images in raw format, can basically be used as three-band radiometers (Red, Green, and Blue, RGB) for water measurements, giving images with pixel values in RGB between 0 and 255 (Goddijn and White 2006; Goddijn-Murphy et al. 2009). Raw image formats are intended to capture as closely as possible the radiometric characteristics of the scene, that is, physical information about the light intensity and color of the scene. The three RGB values can be combined to a set of 256^3 distinct colors. The majority of digital cameras in smartphones deliver images that appear very realistic to the human eye. Nevertheless, these images must be processed before a reliable indication of the intrinsic water color can be derived, because they have been pre-processed from the raw image. Therefore, the analysis must undo the image pre-processing by applying a number of corrections. In this study, the camera provides a widely adopted standard format: the standard RGB color space (referred as *sRGB*), with a gamut (range of colors) considerably smaller than the human eye vision (Reinhard et al. 2007). The most important corrections for the *sRGB* format are the “Gamma” and “Illumination” corrections, which are described in more detail below. In this article, we follow the conventions as laid out by the International Color Consortium (ICC 2014) that has defined an open source color management system that allows smooth communication on color transformations between photography, printing and painting.

Gamma correction

The human eye is more sensitive to relative differences in brightness in the darker tones of an object, while the camera is almost linear in the conversion of luminance to the digital number (DN). The *sRGB* format accommodates this aspect by applying the Gamma compression

$$V_{\text{out}} = V_{\text{in}}^\gamma \quad (3)$$

where V_{out} is the output luminance value and V_{in} is the actual luminance value, and γ is the gamma value. The gamma value is usually between 0.5 and 0.35, over the interval [0 1] that has the effect of enhancing contrast at the lowest luminosity levels and reducing the contrast at the highest levels (Wyszecki and Stiles 1982).

The inverse procedure (Gamma expansion) restores the digital numbers to a linear level. The DN in the three channels of the *sRGB* output are combined in the vector **S**. First each channel is normalized to the interval [0 1] and subsequently for all values above 0.04045 the Gamma expansion is applied to derive the linear color vector **L** (for values below 0.04045 the expansion is not applied, see Westland et al. 2012):

$$\mathbf{L} = ((\mathbf{S}/255 + 0.055)/1.055)^\gamma \quad (4)$$

A simple test was completed in the laboratory, where the Gamma-function of a NIKON D60 and a Samsung EK-GC100 camera were checked, following procedures found in literature (Reinhard et al. 2007). A prepared panel from Munsell standards (ASTM D1535-68; Munsell 1912) that contained 10 Grey cards with well-known albedo (between 15% and 90%) and illuminated by the D65 lamps in a lighting cabinet (VeriVide, width: 600 mm, 20 W) was photographed (no flash) and the radiance was measured with a Photo Research PR655 spectrometer. For each grey surface the DN in each of the three channels was recorded and plotted against the albedo. This experiment showed mainly that for the Samsung EK-GC100 and the NIKON camera the three colors (RGB) follow the same compression with γ near 2.2 and 2.0 respectively, although one simple value could not describe the compression for all values. Since the NIKON is a reflex SLR camera providing values in raw format we assumed the difference relied on the type of camera. Since the *sRGB* color space standard used with most cameras, PCs, and printers has a decoding gamma value near 2.2 over much of its range, we applied this decoding value for all the images analyzed on a first step. Testing of gamma values for additional cameras was not possible for this study, but the point of this exercise was to show the existence of differences between types of cameras and indicate that this could be a source of dissimilarities between color calculations. If this is the case, an adaptation of the gamma value for the camera used could improve the color estimates.

sRGB to tristimulus

The Commission Internationale de l’Eclairage (CIE 1931) introduced colorimetry as “a system for color measurements” and created “CIE 1931 XYZ color space” (Wright 1928; Thomas and Guild 1931; Guild 1932; Fairman et al. 1997). This color space includes all the colors that an average person can experience. It works as a standard reference against which many other color spaces are defined and forms the basis for nearly all applied colorimetry. The white point (also referred as achromatic point) is a set of chromaticity coordinates that serve to define the color “white” in a color space. These coordinates can change depending on the illumination characteristics. In the camera the output of the photon detection system is already converted to *sRGB* values, based on detailed laboratory measurements of the wavelength

dependence of the three channels. The *sRGB* values are converted to the *XYZ* CIE system (presented by the vector \mathbf{X}') using the matrix \mathbf{M} (Eq. 5).

$$\mathbf{X}' = \mathbf{M} \times \mathbf{L} \quad (5)$$

where the elements of \mathbf{M} are

$$\mathbf{M} = \begin{bmatrix} 0.4124 & 0.3576 & 0.1805 \\ 0.2126 & 0.7152 & 0.0722 \\ 0.0193 & 0.1192 & 0.9505 \end{bmatrix}$$

The values of this matrix were extracted from Pascale (2003), but a detailed description on the calculation of the conversion matrices can be found as well in Wyszecki and Stiles (1982).

Chromatic adaptation

The color perceived by the human eye or detected by a spectrometer or camera depends on the spectral distribution of the light source that illuminates the object. In the CIE (2014), standard illumination conditions have been defined. Examples are D75, D55, and D65 that are representative for daylight illumination in the early morning, midday and average daylight color under clear skies, respectively. The *sRGB* format has adopted a D65 illumination. Therefore, once the signal is corrected for the gamma compression and converted to \mathbf{X}' , a standard illumination correction must take place to transform the color from D65 to E (Equilibrium or the same energy at all wavelengths: white light illumination), given by the vector \mathbf{X} . This procedure also called illumination correction or chromatic adaptation, can be constructed with the help of the so-called *cone response matrix* that takes into account the response (of the human eye) to changes in the perceived colors. A standard chromatic adaptation procedure, well documented in the literature, is applied. In this study, the Bradford method is used, based on the cone response matrix \mathbf{B} (Eq. 6) that allows significant changes in the red-green band overlap (von Kries 1970; Wyszecki and Stiles 1982; Fairchild 2005; Lindbloom 2007–2010).

Elements of \mathbf{B} are:

$$\mathbf{B} = \begin{bmatrix} 0.8951 & 0.2664 & -0.161 \\ -0.7502 & 1.7135 & 0.0367 \\ 0.0389 & -0.0685 & 1.0296 \end{bmatrix} \quad (6)$$

For completeness, the transformations are summarized here. First the source white \mathbf{Ws} and destination white \mathbf{Wd} colors are established and transformed with \mathbf{B} :

$$\mathbf{BWs} = \mathbf{B} \times \mathbf{Ws} \text{ and } \mathbf{BWd} = \mathbf{B} \times \mathbf{Wd} \quad (7)$$

In this case \mathbf{Ws} is given by the D65 illuminant, with elements [0.95047 1.0000 1.08883] and \mathbf{Wd} is given by E with elements [1.000 1.000 1.000]. The illumination correction or

chromatic adaptation calculated to derive the intrinsic color vector \mathbf{X} by applying the illumination correction matrix \mathbf{ICM} :

$$\mathbf{X} = \mathbf{ICM} \times \mathbf{X}' \text{ with } \mathbf{ICM} = \mathbf{B}^{-1} \times (\mathbf{BWd}/\mathbf{BWs}) \times \mathbf{B} \quad (8)$$

In Eq. 8 the \mathbf{B}^{-1} is the inverse matrix of \mathbf{B} and $(\mathbf{BWd}/\mathbf{BWs})$ is a matrix with three diagonal elements $\mathbf{BWd}_i/\mathbf{BWs}_i$ ($i = 1, 2, \text{ or } 3$) and zero for off-diagonal elements.

Water illumination correction

In this study, monitoring of the intrinsic color of natural waters is targeted and therefore a correction must be carried out to compensate for the color of the illumination. In the absence of rain or nearby shadows the following components determine the illumination and the radiation that is measured by the camera.

All components are considered wavelength dependent, with the exception of the Fresnel reflection (ρ) at the air-water interface, which acts as a mirror (specular reflection) where part of the incoming light is reflected. The magnitude of ρ is between 2% and 100%, depending on the incident angle and polarization. The light that is observed by the camera consists of two components: the first component is the light that is scattered in the water column and emerges from the water. The second component is the light from the sky that is reflected at the surface. If Eqs. 1 and 2 are combined, an expression for the upwelling radiance is found:

$$L_{\text{sfc}} = (E_S \times R_{\text{RS}}) + (L_{\text{sky}} \times \rho) \quad (9)$$

Here R_{RS} is the remote-sensing reflectance spectrum that contains the intrinsic color of the water. The wavelength dependence has been omitted in this equation for clarity. We define here the illumination irradiance spectrum E_{ill} ($(\lambda, 0^+)$) as the quantity that modifies the intrinsic color of water to the observed color by the camera:

$$L_{\text{sfc}} \equiv E_{\text{ill}} \times R_{\text{RS}} \quad (10)$$

By combining Eqs. 9 and 10 an expression for E_{ill} can be found:

$$E_{\text{ill}} = (L_{\text{sfc}} \times E_S) / (L_{\text{sfc}} - \rho \times L_{\text{sky}}) \quad (11)$$

This simple equation can be used to reconstruct the illumination correction if E_S , L_{sfc} and L_{sky} are measured and if ρ is known. In the “theoretical” case that ρ goes to zero, the contribution of the sky radiation equals zero and Eq. 10 reduces to $E_{\text{ill}} = E_S$.

For each of the 43 stations sampled the RAMSES spectra of L_{sfc} , L_{sky} and E_S were used to derive E_{ill} according to Eq. 10. For all the measurements made in The Netherlands the below-water spectra and above water spectra compared well when an average ρ of 0.029 was adopted. The E_{ill} spectra were folded with the CIE1931 response curves to give 43

vectors that represent the source white that can be used to derive the illumination matrix for each station, according to Eqs. 6–8.

Hue color angles

The Hue color angle (α_w) for the images were processed according to the previously described image processing steps (Eqs. 1–11). Then the tristimulus values are converted to the CIE chromaticity coordinates using Eq. 12.

The CIE 1931 chromaticity coordinates were calculated according to:

$$x = \frac{X}{X+Y+Z} \text{ and } y = \frac{Y}{X+Y+Z} \quad (12)$$

More information on the calculation of tristimulus values and chromaticity coordinates can be found in Wyszecki and Stiles (1982).

The hue color angle is calculated using the following equation:

$$\alpha_w = \arctan (y_i - y_w, x_i - x_w) \text{ modulus } 2\pi \quad (13)$$

where α_w is the angle to be calculated, and “ $y_i - y_w$ ” and “ $x_i - x_w$ ” are the chromaticity coordinates derived from the images with respect to the white point.

In the case of the spectral measurements acquired in the field, considered as the true or intrinsic color of the water, the spectral curves were transforming to the the tristimulus values XYZ using the reflectance and according to:

$$\begin{aligned} X &= 683 \int_{360}^{830} S(\lambda) \bar{x}(\lambda) \Delta(\lambda) \\ Y &= 683 \int_{360}^{830} S(\lambda) \bar{y}(\lambda) \Delta(\lambda) \\ Z &= 683 \int_{360}^{830} S(\lambda) \bar{z}(\lambda) \Delta(\lambda) \end{aligned} \quad (14)$$

where $S(\lambda)$ is the spectral data that depends on the wavelength (λ), XYZ are the tristimulus values and \bar{x} , \bar{y} , \bar{z} are the CIE color-matching functions (CMFs). These are the spectral response curves for the cone-receptors in the human eye as defined by the CIE. Lumens are converted to watts using the 683 constant.

The FU values were derived according to the previous equations 1–14), a methodology that is explained in Wernand et al. (2010) and Novoa et al. (2013) and where α_w is matched to the FU angles determined for the original FU scale solutions (see Fig. 2).

Sub-image selection

The water illumination, just above the air-water interface, is determined by direct visual solar radiation and its scattering from all directions. Multiple components can contribute, like the sun, sky, clouds, rain and surrounding features like trees

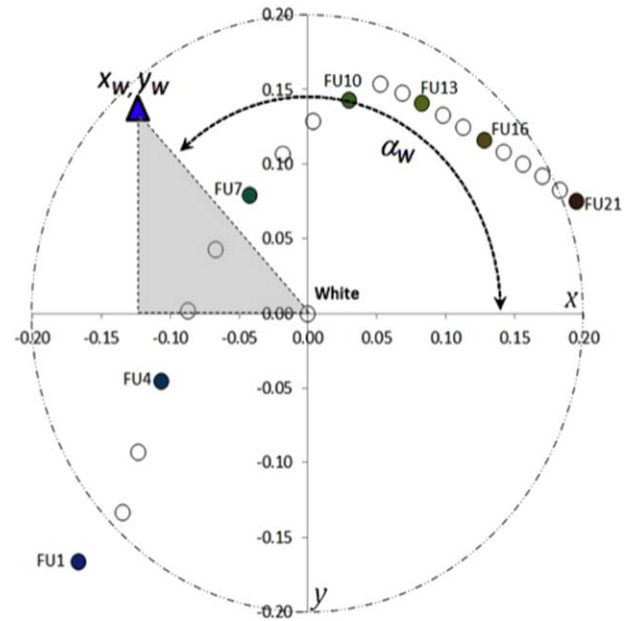


Fig. 2. A chromaticity diagram showing the hue color angle (α_w) match relative to the white point of the scale colors FU1–FU21.

and mountains. But also other local effects may play a role, like the reflection of the hull from nearby boats or shadowing by ramps and jetties. All these components together define the radiation field that illuminates the water. In general, surrounding illumination is wavelength dependent and will influence the color emerging from the water column. It is therefore essential to select the best part of the image where a reliable estimate of the Hue color angle (α_w) can be made.

Images acquired by digital cameras have a large field of view (e.g., The Samsung EK-GC100 has 4608×2592 pixels that cover 60.3 by 42.3°). Because of this, some parts of the images could be more influenced by sky reflectance than other parts. An automated method of selecting the correct part of the image, the part which reveals the “true color of the water body,” is therefore important. However, this can also be challenging as can be observed in the slopes of Fig. 3a, which shows a typical image of the North Sea with highly variable wave slopes and white caps. Figure 3b shows the estimated (α_w) for every pixel in a small sub-section in the lower left corner (red square).

Hence, the final step of the process is the selection of the part of the image where the color of the water can be retrieved with the least influence of surrounding colors and therefore with the highest precision. Accordingly, 8 by 6 sub-sets of the original image with a size of 41×41 pixels are selected in each image and the distribution of the 1681 angles within each sub-pixel is analyzed using percentiles ($P(z)$), where for example $P(95)$ is the Hue color angle of the 95 percentile in the distribution. For WACODI the following rules were adopted:

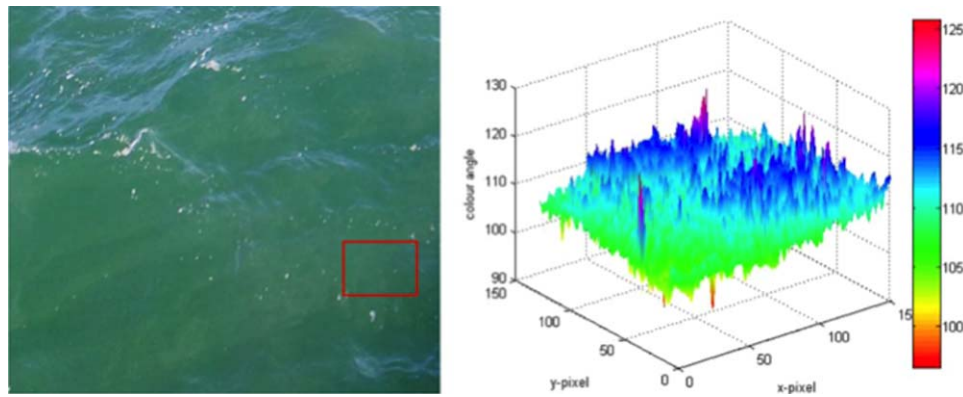


Fig. 3. (a) Photograph taken with a Samsung EK-GC100 GALAXY camera of the North Sea on the 14th of March 2013. (b) Graph of the Hue color angle α_w at pixel level after gamma and illumination correction of the selected sub-image (red rectangle).

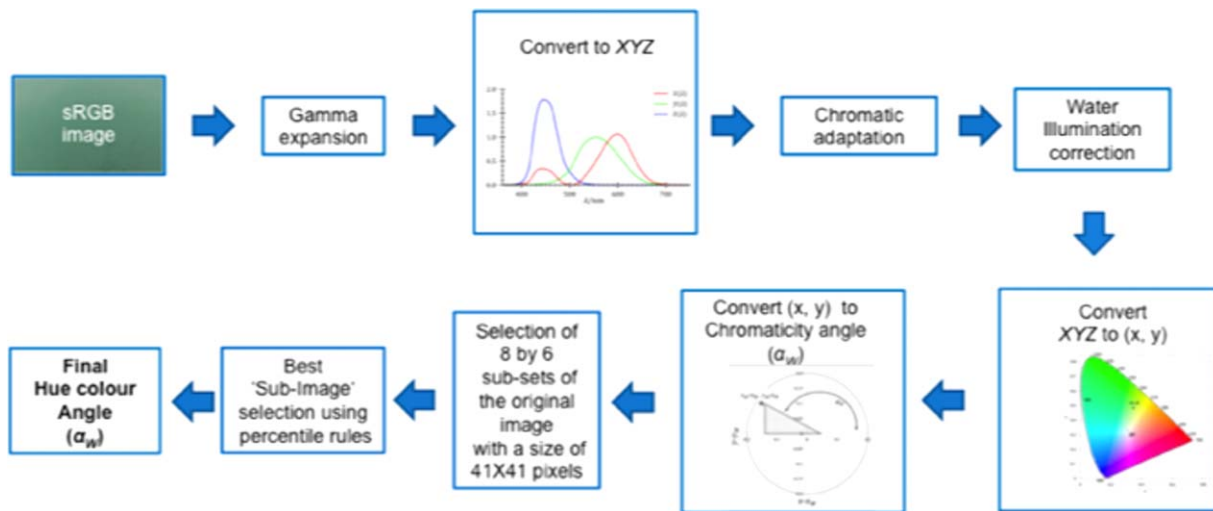


Fig. 4. Summary of the algorithm procedure to extract the intrinsic color of natural waters from *sRGB* images.

1. Natural waters all lie within specific Hue color angle intervals. Only sub-images with that are dominated by water colors are selected; $P(5) > 21^\circ$ and $P(95) < 230^\circ$. If more information on the water body concerned is available, these upper and lower limits may be adjusted.
2. If a flat piece of water without whitecaps and relatively close to the observer is selected, the viewing and illumination geometry should be stable and all angles should fall in a narrow interval around the median. Only sub-images were selected with: $P(90) - P(10) < \Delta$, where Δ can be chosen as a small number (here 4°). To exclude artificial objects in the sub-image, a lower boundary is also adopted: $P(90) - P(10) > 0.8^\circ$.
3. When the chromaticity coordinates (x, y) are very close to the white point, the derivation with the WACODI algorithm is more sensitive to errors in the illumination correction. This effect is minimized by setting a lower limit

to the distance to the white point (saturation), thereby requesting more color expression. This was done by requiring that the median of the saturation distance has to be larger than 0.02.

4. Finally, the minimum of the $P(50)$ values of all sub-sections that comply with these criteria is selected. The reason is that the illumination correction is carried out for a minimum reflection at the surface ($\rho = 0.029$ Fresnel Reflection). Smooth water areas that are further away from the observer will have a larger ρ and therefore a larger sky contribution. In case of a blue sky, the $P(50)$ will be bluer, corresponding to a larger color angle.

In summary (see Fig. 4), the image is converted from *sRGB* format to the CIE *XYZ* color space, undergoing first a gamma expansion and an illumination correction using a correction that is specifically derived for natural waters. After this, the values for each pixel of the image are used to extract the

Table 1. Description of relevant parameters.

Symbol	Units	Description
E_S	$Wm^{-2} nm^{-1}$	Incident spectral irradiance coming from the upper hemisphere
R_{RS}	sr^{-1}	Remote sensing reflectance
L_{sky}	$Wm^{-2}nm^{-1} sr^{-1}$	Downward radiance from the sky
L_{sfc}	$Wm^{-2}nm^{-1} sr^{-1}$	Upward radiance that is measured by the Smartphone
L_W	$Wm^{-2}nm^{-1} sr^{-1}$	Water leaving radiance
ρ	-/-	Fresnel reflection at the water surface
γ	-/-	Gamma coefficient
E_{ill}	$Wm^{-2} nm^{-1}$	Illumination
α_w	Degrees (radians)	Hue color angle for the intrinsic color of a water body

chromaticity coordinates and finally a sub-section is selected, by means of percentiles, to derive the “best” estimate of the intrinsic Hue color angle of the water (α_w). See Table 1 for acronym description.

Results

Field conditions

The water bodies and the weather conditions covered during the two campaigns allowed for testing the WACODI algorithm for a wide range of water colors and illuminations. The concentrations of the water quality indicators varied considerably among the 43 stations, reflecting the widely different water body types that were sampled: central North Sea, coastal North Sea, rivers, lakes and even CDOM- dominated waters (peat lakes), see Table 2 for a summary.

As anticipated, the sky radiance spectra showed very different shapes for sunny conditions (very little or no clouds) compared to overcast skies, notably showing a higher peak in the blue part of the spectrum (~400 nm) in the first case. The downwelling irradiance (E_s) showed very similar shapes for both sky conditions, with a remarkable difference in magnitude (Fig. 5).

From the collected E_S , L_{sky} and L_{sfc} spectra (shown in Fig. 5), the remote sensing reflectance was calculated between 400 and 800 nm according to Eqs. 1 and 2. The variability in spectral shapes, due to a wide variability in the absorbing and scattering substances in the water is illustrated in Fig. 6. Also, color assessments via the in situ Forel-Ule methodology showed a large dynamic range (FU6–FU19).

Table 2. Concentration ranges of water quality indicators (Chl *a*, TSM and CDOM) and Forel-Ule index (FU) measured during the North Sea and the Netherlands campaigns.

	No. of stations	Chl <i>a</i> ($mg m^{-3}$)	TSM ($g m^{-3}$)	CDOM at 440 nm (m^{-1})	FU
North Sea	27	0.54–3.78	0.45–3.06	–	6–13
Netherlands	16	2.36–55.05	1.24–23.94	0.47–3.08	9–19

Illumination correction procedure

The R_{RS} derived from Eq. 2 and multiplied by the CIE1931 sensitivity curves provided the color angle (α_w) following Eqs. 12–14. This is referred to as the intrinsic color or true color of the stations. Also, E_{ill} was first calculated as a function of wavelength by Eq. 10 and then converted to the XYZ color vector that served as W_s (Eqs. 6, 7). Since no digital camera observations were available that covered exactly the same spot of water and operated at exactly the same time (within 0.1 s of the spectrometers), a forward and inverse simulation was carried out.

The L_{sfc} was first converted to an XYZ vector. The Y-signal (luminance) was normalized to a value between 100 and 150 to simulate the camera adaptation of the integration time to reach a DN midway between 0 and 255. The vector was converted to *sRGB* standards (XYZ to *sRGB* and inverse Gamma correction) and converted to 8 bits digital numbers. This vector was analysed and converted from *sRGB* to a color angle of that pixel by the WACODI gamma and illumination processing software (SIM).

In Fig. 7, a histogram is shown of the difference in color angle between true and the simulation outcome (R_{RS} -SIM). The histogram shows that 68 out of 71 simulations resulted in a color angle less than 5° from the true color. The median indicates and overall offset of minus 1.1° and 76% of the observations is found within 2° from the original. The distribution is skewed and 90% of the observations (5–95 percentile) is found between 0.6° and –4.6°. Given that the average angle difference between FU color values is 10°, this offset is not considered to be significant in most cases, except for FU colors 20 and 21, which show an angle difference of 4° (see Novoa et al. 2013, 2014 for additional information on the FU scale).

The outcome of this simulation is a proof of concept of the illumination correction along the lines of CIE (2014) written in terms of vectors and illumination correction matrices. In case this correction creates a large offset, we can quite easily identify in the original spectra the issue, such as the effects of rapidly changing condition near clouds.

Image processing with WACODI

The WACODI algorithm was run on the images acquired at each of the 43 stations that were visited during the North Sea and the Netherlands campaigns. The images acquired showed a wide color range from blue-green to brown (see examples in Fig. 8). In most cases, only the water surface

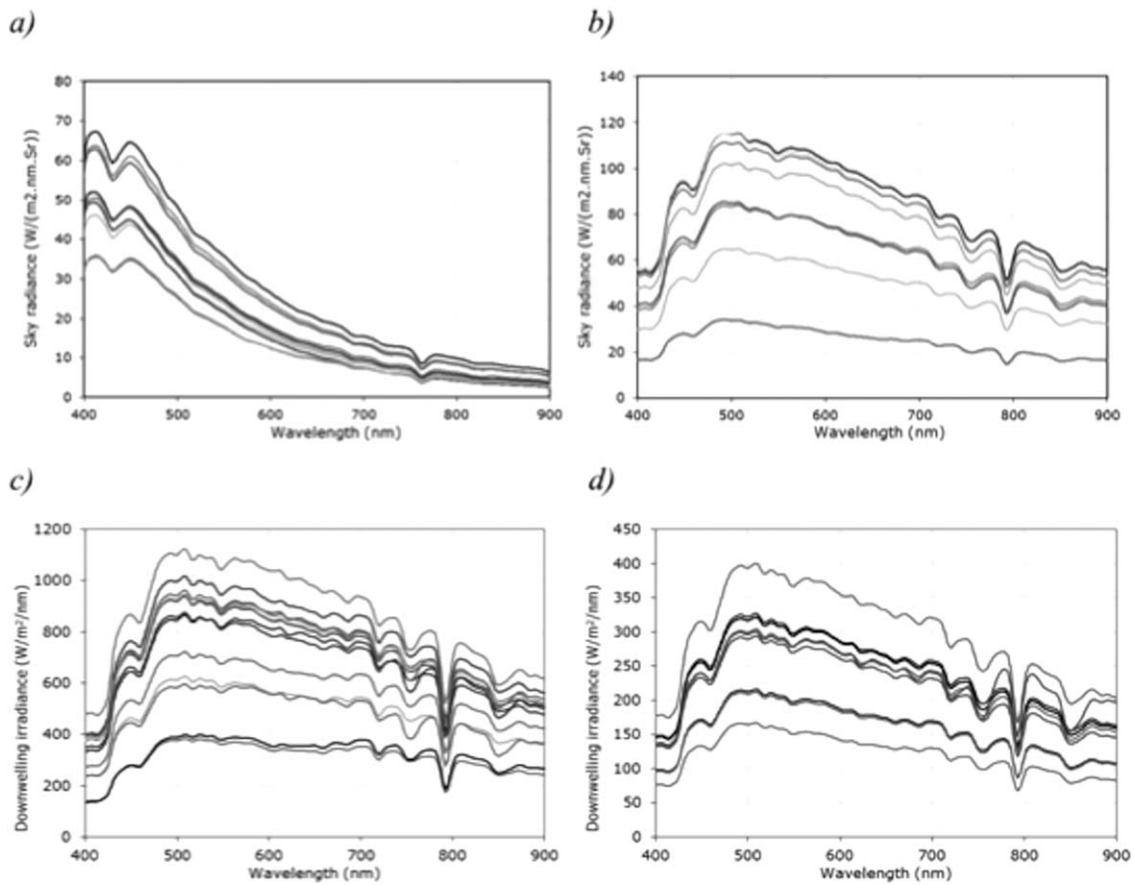


Fig. 5. Sky radiance spectra (top) and incident spectral (downwelling) irradiance (bottom) measured during the North Sea and Netherlands campaigns under sunny (a, c) and overcast (b, d) conditions.

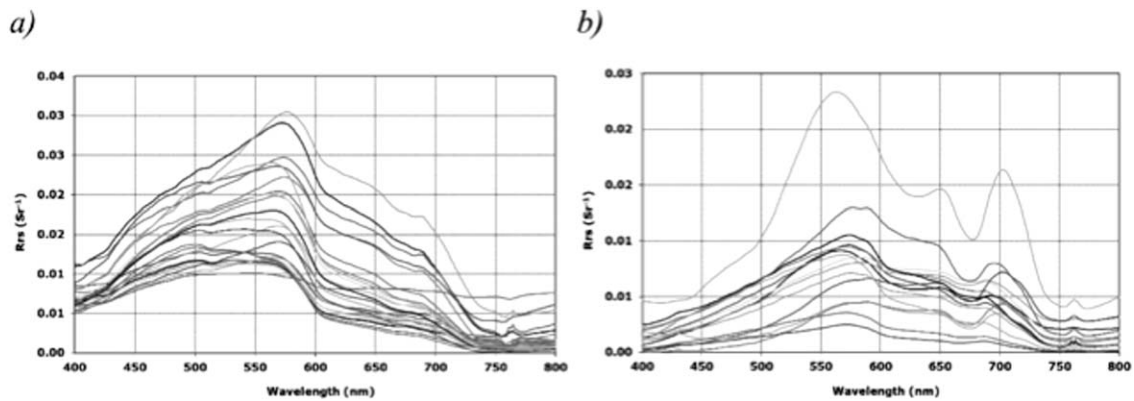


Fig. 6. Remote sensing reflectance spectra of the 43 stations sampled during both the North Sea (a) and the Netherlands (b) field campaigns.

was visible on the images, but in some cases objects were visible.

As measurements of the radiation field above and below water were conducted, independent information was available on the intrinsic color of the water and on the vector that was used in the illumination correction. The regression

between the α_w extracted using radiometric data and extracted from digital imaging shows a coefficient of determination of $r^2 = 0.93$ and most of the 43 images fall close to the 1: 1 line as can be appreciated in Fig. 9. Station 15 is represented twice, once when the part of the sub-image is selected using the minimum P(50) value and the other when

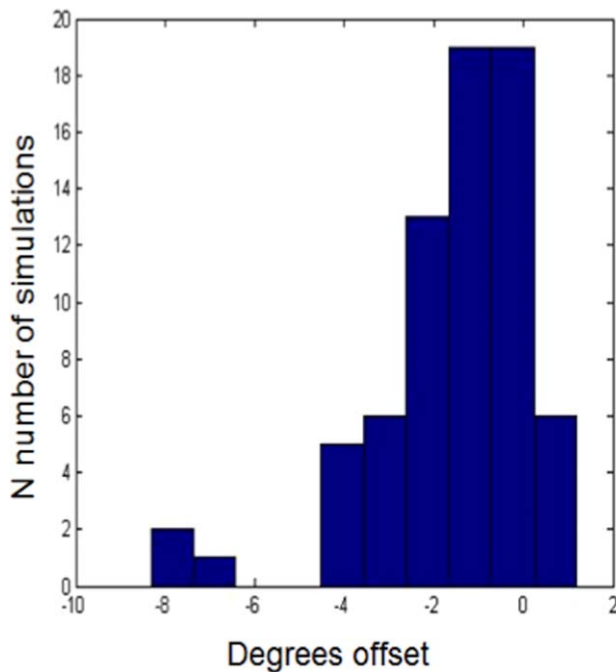


Fig. 7. Frequency histogram of the difference in the Hue color angle between the color of R_{RS} and the color based on the L_{sfc} and illumination correction in degrees.

the center part of the image is selected. In the first case, there is a large offset. However, when the R_{RS} was compared to the image α_w extracted from the center part of the image, the difference notably decreased.

Subsequently, an investigation was made on how WACODI performs in conditions when only the digital image is available and the detailed spectroscopic information on the illumination conditions is missing. The illumination conditions were divided into two categories: overcast and sunny. For scattered cloud conditions ($CC < 4/8$), the values for sunny weather conditions were assigned for that image.

The chromaticity coordinates (x, y) of the illumination vector E_{ill} extracted for both categories are shown in Fig. 10. Notice that the coordinates for sunny conditions appear far less dispersed than the coordinates for the overcast conditions. This suggests that there is an easier illumination correction for pictures acquired under clear skies, as there is a lower variability of the coordinates used for the correction. Two generic illumination vectors E_{ill} were derived from the median values for either overcast or sunny weather conditions (sunny and overcast median values, Fig. 10). The vectors have elements [0.96 1.00 0.99] and [0.98 1.00 1.05], respectively.

When the same dataset was analyzed with either of these two illumination corrections, the dispersion of the regression increased ($r^2 = 0.80$ vs. $r^2 = 0.93$), while the slope of the regression line showed little variation (1.06 vs. 0.98), see Fig. 11. This suggests that a standard correction could be

applied to images, if the sky conditions at the time of the acquisition are known. Higher data dispersion in the greater Hue color angle values (around 100 and 150) can be observed in Fig. 11, which can be attributed to stations that presented scattered clouds at the time of the measurement.

Application of the algorithm to images acquired using the smartphone APP

By December 2014 a total of 64 images of water bodies were acquired using different smartphone brands including Samsungs EK-GC100, GT-I9305, GT-I8190, LG Nexus, Motorola XT1032, Alcatel 6040D and Sony experia. The comparison between the FU estimated using the modern Forel-Ule scale (Novoa et al. 2014) and the FU derived from the image, shows a good correlation as shown in Fig. 12. It can be noticed that there is a higher dispersion in the darker colors 13–21. This could be due to lower hue color angles difference existing between the brownish colors (see Fig. 2).

Discussion and conclusions

The aquatic environment of inland and coastal waters is characterized by a complex mix of natural and anthropogenic influences and ecosystem response. In order to enhance understanding and managing practices of this dynamic environment a monitoring practice that provides good spatial and temporal coverage at low cost is required. This can be partially realized through citizens' effective participation in environmental monitoring through the use of existing devices, such as smart phones, as sensors (www.cit-clops.eu). In this study, we have investigated if digital imagery from cameras in smart phones can be used for monitoring the intrinsic color of natural water bodies.

The water Hue color angle (α_w) is introduced as a simple measure to quantify the spectral distribution of the water leaving radiance. Based on extensive field work we proved that (α_w) can be extracted from $sRGB$ digital images without bias. The extraction was done by a number of steps that included gamma expansion, chromatic adaptation and image processing. The recipe of this processing, called WACODI, is explained in detail in this article. WACODI represents a large improvement with respect to the work conducted by Klaveness (2005), who concluded that digital cameras could only be used to document visual color differences in a qualitative way. Our findings are in agreement with other authors (Goddijn and White 2006; Goddijn-Murphy et al. 2009; Hoguane et al. 2012) who demonstrated that digital cameras can be used to extract quantifiable results, since they were able to correlate RGB values to the concentration of water constituents, such as Chl *a*.

During this study a number of problems were encountered that need more attention in future work. These problems cover surface roughness, illumination conditions, white balance, and sub-image selection.

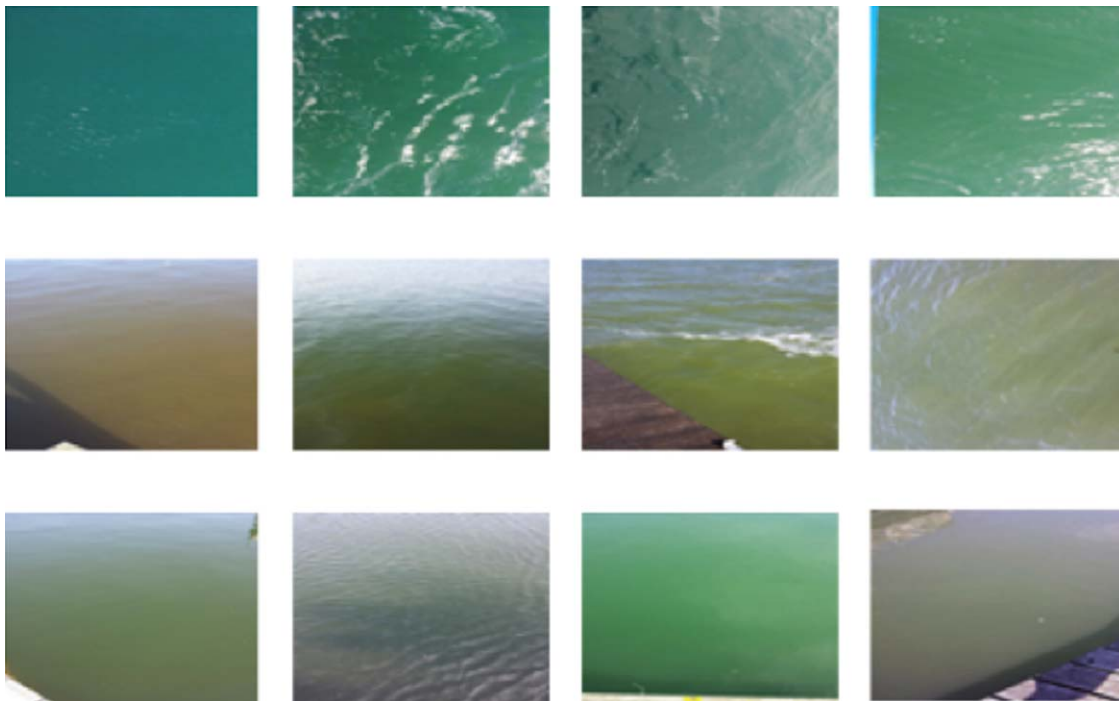


Fig. 8. A selection of images used for the determination of the intrinsic color. Top four images correspond to North Sea waters. The rest of the images correspond to Dutch inland waters.

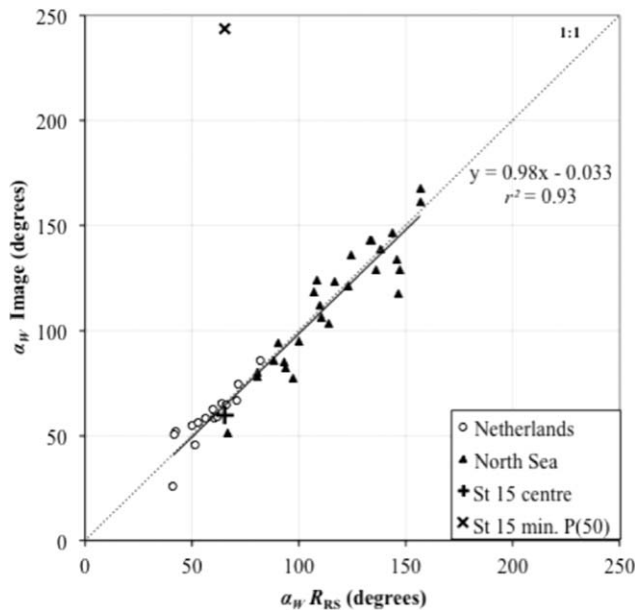


Fig. 9. Correlation between Hue color angles (α_w) derived from both R_{RS} spectra against sRGB images corrected for the illumination (section sRGB to Tristimulus) to each station.

Surface roughness

The boundary between air and water acts as a mirror that reflects the incoming sky radiance into the camera. Although the efficiency of reflection is generally small (a few percent)

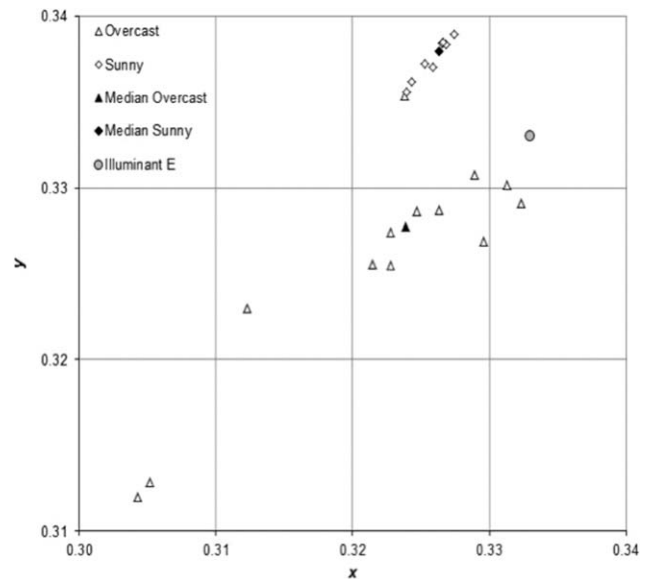


Fig. 10. Illumination chromaticity coordinates (x, y) derived for overcast and sunny sky conditions.

it provides a large and highly variable contribution to the total measured radiance, since natural waters also have a small remote sensing reflectance value (Mobley 1999). WACODI has included the correction for this surface reflection in the illumination correction matrix. Especially in clear sky conditions, when the illumination has a very blue

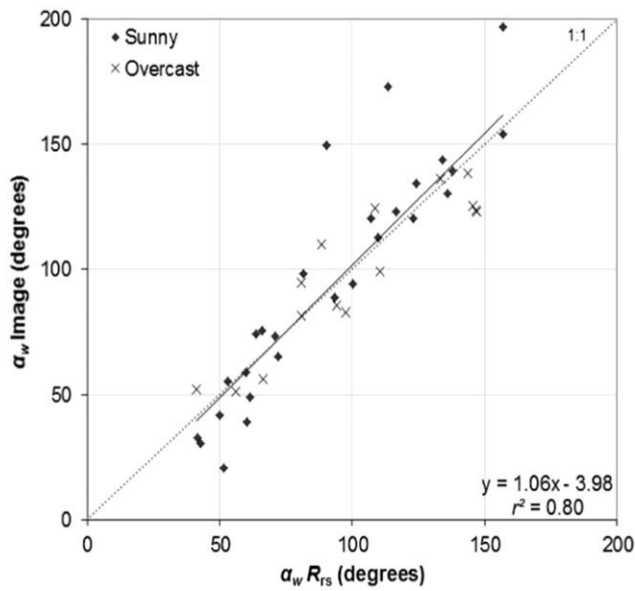


Fig. 11. Correlation between Hue color angles (α_w) derived from reflectance spectra (R_{RS}) and from *sRGB* images applying a two-case illumination correction; one for overcast and one for sunny/clear/scattered cloudy skies.

characteristic color, this can have a large impact on the retrieved α_w when the size of this contribution is over (-under) estimated. In this respect Fig. 3b is very intriguing, showing a pixel-to-pixel variability in α_w that could be a combination of intrinsic variation in water composition and complex surface roughness due to capillary waves.

Illumination conditions

In the general case where an image is acquired without detailed spectrophotometric measurements, but the sky condition is known (either overcast or sunny) the estimation of water color still can be accomplished, but with less precision. Examining the regression graph in Fig. 11, more dispersion can be observed in the higher Hue color angle values (around 100 and 150) away from the 1: 1 line, which can be attributed to stations that presented scattered clouds at the time of the measurement. To improve the results, the same test was completed with three categories (i.e., overcast, sunny, and scattered clouds), introducing the median chromaticity coordinates derived from all the stations classified as “scattered skies,” but the relationship did not improve. This was due to the high variability of illumination conditions caused by the clouds, making the median values of this category not appropriate. If cloud covers are changing fast it is more difficult to estimate the right illumination at the exact moment of image acquisition. Our recommendation to overcome this problem is to use pictures acquired under clear skies to derive an accurate Hue color angle, because the illumination correction values are more stable for this condition.

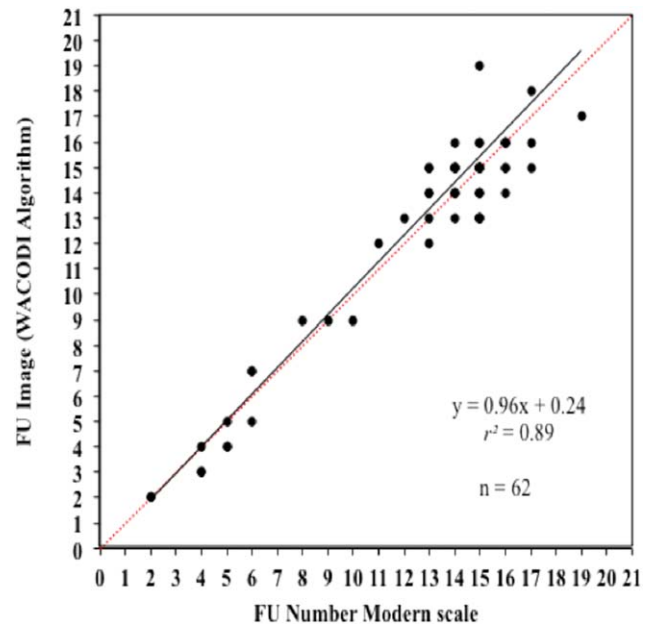


Fig. 12. Scatter plot showing the correspondence between FU values calculated using the hue color angles derived from digital images sent by the public and the corresponding FU values assessed visually by the users using the modern Forel-Ule scale.

White balance

During this study the images were acquired as close to the water as possible, to ensure correct white balancing. The white-balance setting attempts to mimic the natural color adaptation performed by human eyes. This setting adjusts the color of the pixels under different illuminations, using algorithms to identify the neutral tones in the photo (the whites, greys, and blacks) and then calibrate the rest of the image to the temperature of the neutral colors (Buchsbaum 1980; Hung 2005). This is an advantage for the user since it is easy and simple to take the picture, however it can cause problems in certain conditions, especially when objects other than the water and neutral grey/white tones are included in the picture.

A widely adopted algorithm is the Grey World Assumption (Buchsbaum 1980), which usually works reasonably well in natural scenes (Jiang et al. 2012). In this study, this setting did not present issues when the photographs were taken correctly, however, when the analysis was applied to certain images during the campaign that were taken without following the protocol precisely, the results were less successful, illustrating the importance of a correct image acquisition procedure. If future technological developments allow it, low-cost cameras will all soon incorporate several white balance and a raw format options that could be used to improve the procedure presented in this document (*see* also Goddijn-Murphy et al. 2009). In addition, differences in white balance procedures should be assessed among the most common smartphone and digital camera brands used

in the market, to standardize the procedure. Further studies and algorithm developments should consider the direct sunlight settings to standardize the images or, for example, to take the images using the flash as it would probably affect only some pixels of the image that could be used to normalize the others.

Sub-image selection

The sub-image selection process presented here provided better results compared to other selections criteria tested, for instance selecting the center part of the image analyzed, except for one case: The station located in Markermeer De Hemmelanden, an inland marina (See the bottom right image on Fig. 8). The RAMSES spectra measured at this station are very stable and similar. Two images were taken close to the jetty and gave identical results, even if they were taken 30 min apart. However, the situation at the jetty was very different from other stations, because the jetty was surrounded by boats and boat ramps, so probably there is a shading effect taking place on the image that was not captured by the radiometric data. Likely, the sky radiation was blocked by nearby boats and did not contribute to the illumination of the water surface. Thereby, the blue light was overcorrected, resulting in a bluer color. The minimum P(50) value selected at the end of the process most likely chose the darker part on the image, but when the center part was selected, the difference between the R_{RS} derived angle α_w and the image derived angle α_w is low (α_w from $R_{RS} = 65$; α_w from image = 59.8). Hence, this issue indicates there should not be shades of objects present on the water surface at the moment the image is captured.

The comparison between the FU estimated with the Modern Forel-Ule scale (considered as the groundtruth value) and the FU derived from images acquired using different smartphones, shows a good match, which is promising, however a higher number of contributions is necessary to evaluate the algorithm's performance. Our objective with this manuscript was to provide the possibility to use this algorithm to extract the Hue color angle from digital images. The MATLAB® routine to apply this WACODI algorithm is available as Supporting Information.

References

- Anderson, D. M., P. M. Glibert, and J. M. Burkholder. 2002. Harmful algal blooms and eutrophication: Nutrient sources, composition and consequences. *Estuaries* **25**: 704–726. doi:10.1007/BF02804901
- Arar, E. J. 1997. EPA Method 446.0 In vitro determination of chlorophylls a, b, c + c and pheopigments in marine and freshwater algae by visible spectrophotometry, Revision 1.2 in: EPA/600/R-97/072. Methods for the determination of chemical substances in marine and estuarine environmental matrices. EPA US.
- ASTM D1535-68. 1969. Specifying color by the Munsell system, p. 255. American Society for Testing Materials.
- ASTM E308. 1999. Standard practice for computing the colors of objects by using the CIE system, p. 44. American Society for Testing Materials.
- Blondeau-Patissier, D., G. H. Tilstone, V. Martinez-Vicente, and G. F. Moore. 2004. Comparison of bio-physical marine products from SeaWiFS, MODIS and a bio-optical model with in situ measurements from Northern European waters. *J. Opt. A Pure Appl. Opt.* **6**: 875–889. doi:10.1088/1464-4258/6/9/010
- Bøgestrand, J., P. Kristensen, and B. Kronvang. 2005. Source apportionment of nitrogen and phosphorus inputs into the aquatic environment. Report 7. European Environment Agency. European Environment Agency. ISSN 1725-9177.
- British Columbia Ministry of Environment. 1999. Government, Canada. Environmental protection division. Approved Water Quality Guidelines Report [accessed on 2015 October 1]. Available from www.env.gov.bc.ca/wat/wq/BCguidelines/color/color_over.html
- Buchsbaum, G. 1980. A spatial processor model for object color perception. *J. Franklin Inst.* **310**: 1–26. doi:10.1016/0016-0032(80)90058-7
- CIE. International commission on Illumination. 2014. <http://www.cie.co.at/index.php/Publications> [last accessed January 2015]
- Davies-Colley, R. J., W. N. Vant, and D. G. Smith. 1993. Colour and clarity of natural waters. Ellis Horwood Limited.
- Davies-Colley, R. J., D. G. Smith, D. J. Speed, and J. W. Nagels. 1997. Matching natural water colors to Munsell standards. *J. Am. Water Resour. Assoc.* **33**: 1351–1361. doi:10.1111/j.1752-1688.1997.tb03558.x
- Deschamps, P.-Y., B. Fougnie, R. Frouin, P. Lecomte, and C. Verwaerde. 2004. SIMBAD: A field radiometer for satellite ocean-color validation. *Appl. Opt.* **43**: 4055–4069. doi:10.1364/AO.43.004055
- Dyer, K. R., and T. J. Moffat. 1998. Fluxes of suspended matter in the East Anglian plume Southern North Sea. *Cont. Shelf Res.* **18**: 1311–1331. doi:10.1016/S0278-4343(98)00045-4
- Eleveld, M. A., R. Pasterkamp, H. J. van der Woerd, and J. D. Pietrzak. 2008. Remotely sensed seasonality in the spatial distribution of sea-surface suspended particulate matter in the southern North Sea. *Estuar. Coast. Shelf Sci.* **80**: 103–113. doi:10.1016/j.ecss.2008.07.015
- Fairchild, M. D. 2005. Color appearance models, p. 1–409. Wiley.
- Fairman, H. S., M. H. Brill, and H. Hemmendinger. 1997. How the CIE 1931 color-matching functions were derived from Wright-Guild Data. *Color Res. Appl.* **22**: 11–23. doi:10.1002/(SICI)1520-6378(199702)22:1 <11::AID-COLA>3.0.CO;2-7
- Ferreira, J. G., and others. 2011. Overview of eutrophication indicators to assess environmental status within the European Marine Strategy Framework Directive. *Estuar. Coast. Shelf Sci.* **93**: 117–131. doi:10.1016/j.ecss.2011.03.014

- Forel, F. A. 1895. Le Léman, Monographie Limnologique II, p. 651. Librairie de l'Université, Lausanne.
- Giardino, C., V. E. Brando, A. G. Dekker, N. Strömbeck, and G. Candiani. 2007. Assessment of water quality in Lake Garda (Italy) using Hyperion. *Remote Sens. Environ.* **109**: 183–195. doi:10.1016/j.rse.2006.12.017
- Goddijn, L. M., and M. White. 2006. Using a digital camera for water quality measurements in Galway Bay. *Estuar. Coast. Shelf Sci.* **66**: 429–436. doi:10.1016/j.ecss.2005.10.002
- Goddijn-Murphy, L., D. Dailloux, M. White, and D. Bowers. 2009. Fundamentals of in situ digital camera methodology for water quality monitoring of coast and ocean. *Sensors* **9**: 5825–5843. doi:10.3390/s90705825
- Gohin, F., and others. 2005. Satellite-derived parameters for biological modelling in coastal waters: Illustration over the eastern continental shelf of the Bay of Biscay. *Remote Sens. Environ.* **95**: 29–46. doi:10.1016/j.rse.2004.11.007
- Guild, J. 1932. The colorimetric properties of the spectrum. *Philos. Trans. R. Soc. Lond. Ser. A* **230**: 149–187. doi:10.1098/rsta.1932.0005
- Heisler, J., and others. 2008. Eutrophication and harmful algal blooms: A scientific consensus. *Harmful Algae* **8**: 3–13. doi:10.1016/j.hal.2008.08.006
- Hoguane, A. M., C. L. Green, D. G. Bowers, and S. Nordez. 2012. A note on using a digital camera to measure suspended sediment load in Maputo Bay, Mozambique. *Remote Sens. Lett.* **3**: 259–266. doi:10.1080/01431161.2011.566287
- Hu, C., Z. Chen, T. D. Clayton, P. Swarzenski, J. C. Brock, and F. E. Muller-karger. 2004. Assessment of estuarine water-quality indicators using MODIS medium resolution bands: Initial results from Tampa Bay, FL. *Remote Sens. Environ.* **93**: 423–441. doi:10.1016/j.rse.2004.08.007
- Hung, P.-C. 2005. Color theory and its application to digital still cameras, p. 205–221. In Junichi Nakamura [ed.], *Image sensors signal process digit still cameras*. CRC Press.
- IOCCG. 2000. Remote sensing of ocean color in coastal, and other optically-complex waters, p. 144. In S. Sathyendranath [ed.], *Reports of the International Ocean-Colour Coordinating Group 3*. IOCCG Project Office, Dartmouth, Canada.
- IOCCG. 2008. Why ocean color? The societal benefits of ocean-color technology, p. 141. In T. Platt, N. Hoepffner, V. Stuart and C. Brown [eds.], *Reports of the International Ocean Color Coordinating Group 7*. Dartmouth, Nova Scotia, B2Y 4A2, Canada.
- Jeffrey, S. W., and M. Vesk. 1997. Introduction to marine phytoplankton and their pigment signatures. In S. W. Jeffrey, R. F. C. Mantoura and S. W. Wright [eds.], *Phytoplankton pigments in oceanography: Guidelines to modern methods*. United Nations Educational Scientific and Cultural Organization (UNESCO).
- Jiang, J., Y. Zhao, and S. Wang. 2012. Color correction of smartphone photos with prior knowledge. *Proc. SPIE* **8302**, Imaging and Printing in a Web 2.0 World III, 83020H (21 February 2012); 1–6. doi:10.1117/12.910137
- Kallio, K., T. Kutser, T. Hannonen, S. Koponen, J. Pulliainen, J. Vepsäläinen, and T. Pyhälähti. 2001. Retrieval of water quality from airborne imaging spectrometry of various lake types in different seasons. *Sci. Total Environ.* **268**: 59–77. doi:10.1016/S0048-9697(00)00685-9
- Klaveness, D. 2005. Photography in limnology: Documentation of lake color using a CCD camera. *Limnology* **6**: 131–136. doi:10.1007/s10201-005-0147-8
- Lindbloom, B. 2007–2010. Section: Math, Chromatic adaptation. Available from www.brucelindbloom.com. [accessed jan 2015].
- McManus, J. P., and D. Prandle. 1997. Development of a model to reproduce observed suspended sediment distributions in the southern North Sea using principal component analysis and multiple linear regression. *Cont. Shelf Res.* **17**: 761–778. doi:10.1016/S0278-4343(96)00057-X
- Mobley, C. D. 1999. Estimation of the remote-sensing reflectance from above-surface measurements. *Appl. Opt.* **38**: 7442–7445. doi:10.1364/AO.38.007442
- Mueller, J. L., and others. 2003. NASA/TM-2003-Ocean optics protocols for satellite ocean color sensor validation, Revision 4, vol. III: Radiometric measurements and data analysis protocols. Revision. National Aeronautical and Space administration Goddard Space Flight Space Center Greenbelt, Maryland.
- Munsell, A. H. 1912. A pigment color system and notation. *Am. J. Psychol.* **23**: 236–244. doi:10.2307/1412843
- Nechad, B., K. G. Ruddick, and Y. Park. 2010. Calibration and validation of a generic multisensor algorithm for mapping of total suspended matter in turbid waters. *Remote Sens. Environ.* **114**: 854–66. doi:10.1016/j.rse.2009.11.022
- Novoa, S., G. Chust, Y. Sagarminaga, M. Revilla, A. Borja, and J. Franco. 2012. Water quality assessment using satellite-derived chlorophyll-a within the European directives, in the southeastern Bay of Biscay. *Mar. Pollut. Bull.* **64**: 739–750. doi:10.1016/j.marpolbul.2012.01.020
- Novoa, S., M. R. Wernand, and H. J. van der Woerd. 2013. The Forel-Ule scale revisited spectrally: Preparation protocol, transmission measurements and chromaticity. *J. Europ. Opt. Soc. Rap. Public.* **8**, **1303**:1–8. doi:10.2971/jeos.2013.13057
- Novoa, S., M. R. Wernand, and H. J. van der Woerd. 2014. The modern Forel-Ule scale: A 'do-it-yourself' colorcomparator for water monitoring. *J. Eur. Opt. Soc. Rapid Publ.* **9**: 14025–1:10. doi:10.2971/jeos.2014.14025
- Pascale, D. 2003. A review of RGB color spaces, p. 35. *BabelColor*.
- Reinhard, E., E. Arif Khan, A. Ouz Akyuz, and G. M. Johnson. 2007. *Color imaging: Fundamentals and applications*, Taylor & Francis Inc., USA, p. 1058.
- Smith, R. C., J. E. Tyler, and C. R. Goldman. 1973. Optical properties and color of lake Tahoe and Crater lake. *Oceanography* **18**: 189–199.

- Smith, R. C., and K. S. Baker. 1977. Optical classification of natural waters. Visibility Laboratory. Scripps Institution of Oceanography.
- Thomas, S., and J. Guild. 1931. The C.I.E. colorimetric standards and their use. *Trans. Opt. Soc.* **33**: 73–134. doi: [10.1088/1475-4878/33/3/301](https://doi.org/10.1088/1475-4878/33/3/301)
- Tilstone, G. H., and others. 2002. Regional validation of MERIS chlorophyll products in North Sea REVAMP Protocols, Proceedings of the Working meeting on MERIS and AATSR Calibration and Geophysical Validation (ENVISAT) held in Frascati, 20-24 October 2003, ESA Special Publication WPP-233. p. 77.
- Tudesque, L., M. Gevrey, G. Grenouillet, and S. Lek. 2008. Long-term changes in water physicochemistry in the Adour-Garonne hydrographic network during the last three decades. *Water Res.* **42**: 732–742. doi: [10.1016/j.watres.2007.08.001](https://doi.org/10.1016/j.watres.2007.08.001)
- Ule, W. 1894. Beitrag zur Instrumentenkunde auf dem Gebiete der Seenforschung, Dr. A. Petermanns Mittheilungen aus Justus Perthes geographischer Anstalt **40**: 213–214.
- Ule, W. 1892. Die bestimmung der Wasserfarbe in den Seen, Kleinere Mittheilungen. Dr A Petermanns Mitth aus Justus Perthes Geogr Anstalt. **38**: 70–71.
- Van der Linde, D. W. 1998. Protocol for the determination of total suspended matter in oceans and coastal zones, p. 182. CEC-JRC-Ispra, Tech. note no. I.98.
- Van der Woerd, H. J., and R. Pasterkamp. 2008. HYDROPT: A fast and flexible method to retrieve chlorophyll-a from multispectral satellite observations of optically complex coastal waters. *Remote Sens. Environ.* **112**: 1795–1807. doi: [10.1016/j.rse.2007.09.001](https://doi.org/10.1016/j.rse.2007.09.001)
- von Kries, J. 1970. Chromatic adaptation. In D. Macadam [ed.], *Sources color science*. MIT Press.
- Wernand, M. R., and H. J. Van Der Woerd. 2010. Spectral analysis of the Forel-Ule ocean color comparator scale. *J. Eur. Opt. Soc. Rapid Publ* **5**: 10014s. doi: [10.2971/jeos.2010.10014s](https://doi.org/10.2971/jeos.2010.10014s)
- Wernand, M. R., H. J. Van Der Woerd, and W. W. C. Gieskes. 2013a. Trends in Ocean Colour and Chlorophyll Concentration from 1889 to 2000, Worldwide. *PLoS ONE* **8**: e63766. doi: [10.1371/journal.pone.0063766](https://doi.org/10.1371/journal.pone.0063766)
- Wernand, M. R., A. Hommersom, and H. J. van der Woerd. 2013b. MERIS-based ocean color classification with the discrete Forel–Ule scale. *Ocean Sci.* **9**: 477–487. doi: [10.5194/os-9-477-2013](https://doi.org/10.5194/os-9-477-2013)
- Westland, S., C. Ripamonti, and V. Cheung. 2012. *Computational colour science using MATLAB*. Wiley. ISBN: 978-0-470-66569-5.
- Wright, W. D. 1928. A re-determination of the trichromatic coefficients of the spectral colors. *Trans. Opt. Soc.* **30**: 141–164. doi: [10.1088/1475-4878/30/4/301](https://doi.org/10.1088/1475-4878/30/4/301)
- Wyszecki, G., and W. S. Stiles. 1982. *Color science: Concepts and methods, quantitative data and formulae*, p. 950. Wiley.

Acknowledgments

The authors would like to thank the members of the CITCLOPS consortium who participated in the Netherlands field trip, as well as the crew and scientists on board of the Royal NIOZ RV PELAGIA, for all help provided during the FOKUZ cruise. HJvdW acknowledges prof. A. Dekker for a visitors grant to CSIRO in Canberra, Australia. The research described in this paper is partly supported by the Citclops European project (FP7-ENV-308469). The opinions expressed in this paper are those of the authors and are not necessarily those of Citclops projects partners or the European Commission.

Submitted 22 April 2015

Revised 31 July 2015

Accepted 31 July 2015

Associate editor: Paul Kemp